Journal of Power Sources 223 (2013) 190–198

Contents lists available at SciVerse ScienceDirect

Journal of Power Sources

journal homepage: www.elsevier.com/locate/jpowsour

Synthesis and application of core–shell Co@Pt/C electrocatalysts for proton exchange membrane fuel cells

Rui Lin [a,*], Chunhui Cao [a], Tiantian Zhao [a], Zhen Huang [a], Bing Li [a], Andrzej Wieckowski [b], Jianxin Ma [a,**]

[a] Clean Energy Automotive Engineering Center & School of Automotive Studies, Tongji University, Shanghai 201804, China
[b] Department of Chemistry, University of Illinois at Urbana-Champaign, Urbana, IL 61801, USA

HIGHLIGHTS

- From HR-TEM and XRD test, it was found the core–shell Co@Pt/C structure was formed.
- In-situ XRD was used to trace the nanostructure changes of the catalyst with changing temperature.
- Co@Pt (1:3)/C catalyst exhibited the best catalytic activity toward ORR.
- Performance of single cell kept stable even after 130 h testing.

ARTICLE INFO

Article history:
Received 12 July 2012
Received in revised form
17 September 2012
Accepted 18 September 2012
Available online 28 September 2012

Keywords:
Core–shell structure
Co@Pt/C catalyst
Electrochemical performance
Single cell test
Durability

ABSTRACT

Co@Pt/C core–shell catalysts are synthesized by a two-step chemical reduction method followed by the heat treatment in H_2 and N_2 mixture. High Resolution (HR-TEM), EDX (Energy-dispersive X-ray spectroscopy) and in-situ X-ray diffraction (XRD) techniques are used to characterize the nano-structured catalysts. The results show that the core–shell structure of Co@Pt/C is formed and the average particle size is about 3 nm. From the result of the in-situ XRD, it is found that the heat treatment favors for the formation of crystalline structure and the proper particle size of catalyst. The in-situ XRD detection also helps find the optimized heat treatment temperature. The linear sweep voltammetry (LSV) result reveals that the Co@Pt (1:3)/C (reduced) catalyst exhibits the best catalytic activity toward oxygen reduction reaction (ORR). A 130 h life time test for the single cell, in which the membrane electrode assembly (MEA) using Co@Pt (1:3)/C (reduced) as the cathode catalyst, is operated to evaluate the durability. The results of the test show that the formation of the core–shell structure of Co@Pt/C catalyst is favorable to improve the stability and durability.

1. Introduction

It is well-known that Pt supported on carbon black is normally used as the most active electrocatalyst for oxygen reduction in proton exchange membrane fuel cell (PEMFC) due to its high catalytic activity and excellent chemical stability [1].

While, the challenges caused by the high cost and the limited sources of Pt are preventing PEMFC from widespread application. On the cathode side of the fuel cell, the sluggish reaction kinetics for the oxygen reduction reaction (ORR), which leads to high voltage losses within the fuel cell and therefore causes the low conversion efficiency, has stimulated the researchers to look for the alternative materials that are cheaper and yet perform better or equivalent to the Pt standard [2]. For the purpose of reducing the cost of PEMFC, it is important to develop catalysts with low content Pt but high ORR performance. One way is to alloy Pt with other transition metals such as Fe, Co, Ni and Cr [3]. The promotion of the ORR electro-activity of the Pt-M alloys (M is the transition metals) is attributed to the decrease of the Pt–Pt distance (geometric effect) and the formation of an electronic structure with higher 5d orbital vacancies, which leads to an increase in π electron donation from O_2 to the Pt surface (electronic effect) [4].

However, it is widely reported that Pt-M alloy catalyst is easily de-alloyed and M ions leached into the fuel cell membrane, which would reach to the anode and subsequently electrodeposit there as metallic M film, which will induce to the poison of the membrane [5]. Xu et al. investigated the performance and durability of PtCo alloy catalysts for oxygen electro reduction in acidic environments. PtCo alloy catalysts do not provide long-term improvement in catalytic activity and electrochemical durability due to the leaching

* Corresponding author. Tel.: +86 21 69583837; fax: +86 21 69589121.
** Corresponding author. Tel.: +86 21 69583850; fax: +86 21 69589121.
E-mail addresses: ruilin@tongji.edu.cn (R. Lin), jxma@tongji.edu.cn (J. Ma).

0378-7753/$ – see front matter © 2012 Elsevier B.V. All rights reserved.
http://dx.doi.org/10.1016/j.jpowsour.2012.09.073

of elemental cobalt from the alloys under intensive potential cycling [6]. Carbon supported Pt and Pt–Co nanoparticles were prepared by reduction of the metal precursors. The loss of ORR activity following durability tests was higher in Pt–Co/C than in Pt/C. It can be induced that Pt/C catalyst showed higher electrochemical stability than the binary catalysts [7].

Recently, core–shell structure nanoparticles with transition metals have attracted intense attention owing to their shape-dependent properties and the improvement of the ORR activity. The core–shell nanoparticle catalysts such as M@Pt (M = Cu, Co, Ni, Fe, etc.) for fuel cells have been widely reported. In general, core–shell nanomaterials may be fabricated by combining various types of dielectric materials, metals, semiconductors and pigments, where one material is a core and another or the same material is a shell [8]. This structure is very attractive and might be one of the alternative choices due to its unique properties. The very thin noble metal shell layer over the non-noble metal core can create a particular electronic effect, the so-called strain and ligand effect, of the core substrate on the supported noble metal over layer [9,10]. Core–shell nanostructures are also interesting from the economical point of view because a small amount of expensive material can be used to cover the core made of an inexpensive material [11]. Meanwhile, the formation of core–shell structure can prevent the extensive dissolution of the non-noble metal, a main disadvantage to the alloy catalyst during the fuel cell operation.

In recent researches, Co@Pt nanoparticles are found showing excellent catalytic activity toward ORR. Hence, the development of Co@Pt nanoparticles is not only because of their promising catalytic performance, but also the lower price and greater availability of Co than that of Pt.

Carbon-supported Pt–Co nanoparticles catalysts with core–shell structure were prepared via reduction method and subsequent electrical deposition. It was found that pH values have critical effect on the morphology and activity of the synthesized catalyst. The intrinsic activity of the PtCo/C catalysts for ORR was found to be 2–4 times higher compared with that of Pt/C [12].

The effects of the thickness of the Pt shell, the lattice mismatch, and the particle size on the specific and mass activities from the changes in effective surface area and activity for oxygen reduction induced by stepwise Pt-monolayer depositions on Pd and Pd_3Co nanoparticles was reported [13]. The results suggest that the moderately compressed (111) facets are most conducive to oxygen reduction reaction on small nanoparticles and indicate the importance of concerted structure and component optimization for enhancing the activity and durability of the core–shell structured catalysts.

The nanostructured Co@Pt/C electrocatalysts were prepared by combining the thermal decomposition and the chemical reduction method [14]. The properties of Co@Pt/C electrocatalysts and the kinetics mechanism of the ORR over the Co@Pt/C catalysts were also examined. It was found that the mass activity and specific activity of Co@Pt/C for ORR was superior to that of Pt/C catalyst.

However, the application and the durability of Co@Pt/C catalyst for the fuel cell as well as the formation of core–shell structure were rarely reported. So, in this study, we mainly focused on these topics.

We synthesized carbon supported Co@Pt electrocatalyst by a two-step chemical reduction approach. The morphology characterization was carried out by High Resolution TEM (HR-TEM), Energy-dispersive X-ray spectroscopy (EDX) and in-situ XRD techniques to detect the formation of core–shell structure. And then, the as-prepared Co@Pt/C nanoparticles were applied as cathode catalyst in the single cell. The electro-chemical impedance spectroscopy (EIS), linear sweep voltammetry (LSV) and cyclic voltammograms (CV) technologies were used to detect the electric chemical performance of the catalysts. Also, the durability of the as-prepared catalyst and the single cell was continually operated.

2. Experimental

2.1. Electrocatalyst preparation

Carbon supported Co@Pt catalysts were synthesized through a two-step reduction route. Briefly, the Co particles were prepared by the reduction of cobalt chloride hexahydrate ($CoCl_2 \cdot 6H_2O$, 99%) at the first step [15]. $CoCl_2$ solution (in ethanol, 0.1 M) was mixed with 10 mL polyvinyl alcohol (PVA, repeating units 3000) solution in ethanol which was used as the stabilizer. Then, the freshly prepared sodium borohydride ($NaBH_4$, 97%) solution (in ethanol, 0.05 M) was added dropwise under the vigorous stirring into the mixed solution. To avoid the oxidation of Co nanoparticles, high purity nitrogen (N_2) was kept flowing during the whole procedure. Thirty minutes later, in order to finalize the synthesis of Co nanoparticles, the mixed solution was centrifuged and washed with de-ionized water for several times.

A desired amount of Vulcan XC-72 carbon black (BET surface area: 235 $m^2\ g^{-1}$) which was used as the support material, was ultrasonically dispersed in 30 mL ethylene glycol (EG) for 2 h. Then, the as-synthesized Co particles were dispersed in 20 mL EG and mixed with PVP solution under stirring condition. A stoichiometric amount of dihydrogen hexachloro platinate ($H_2PtCl_6 \cdot 6H_2O$, 99%) solution (in EG, 0.03862 M) was added into the Co mixed hydrosol and followed by careful adjustment of the pH of the mixed solution to 12 with sodium hydroxide (NaOH, 96%) solution (in EG, 2 M).

Then, the suspension was refluxed for 2 h under vigorous stirring. The prepared XC-72 carbon slurry was added into the suspension. The mixture was kept to reflux for 1 h. The mixture was finally adjusted to pH 3 with 5 M hydrochloric acid (HCl) and cooled to room temperature after stirring for 8 h. The powder was separated by filtration and then washed intensively with de-ionized water for times. The washed powder was dried in a vacuum oven at 80 °C for 8 h to obtain the Co@Pt/C catalysts. Finally, in order to reduce Pt and Co and removal the stabilizers, the reduction of the catalyst was performed at reduction atmosphere (5% H_2 and 95% N_2, 40 mL s^{-1}) at 300 °C for 2 h. Co@Pt/C catalysts which were treated under the above conditions were normalized as Co@Pt/C (reduced). Otherwise, the catalyst was normalized as Co@Pt/C.

The weight percent of total metal was 40% of whole catalyst and the molar ratio of Pt:Co is 3 to 1. Co/C nano-particles were also prepared according to the same method for comparison.

2.2. Characterization of the catalyst

2.2.1. Morphology characterization

The morphology of the catalyst particles was observed by the means of TEM analyses with a JEM 2010 EX microscope operating at 200 kV, and the Cu-$K\alpha$ radiation was employed. The structure of the Co-modified Pt/C catalyst was examined by the HR-TEM technique.

XRD (Rigaku Corporation, D/max2550VB3+/PC) was used to measure the crystalline sizes of the catalysts and to verify the existence of Co and Pt elements. The peak was fitted by the Gaussian function to estimate the average particle size, which could be calculated by the Debye–Scherrer equation. The working voltage was 40 kV, and the current was 100 mA, using Cu-$K\alpha$ radiation. Intensity data were collected at 25 °C in the 2θ range 20–90° at a scan rate of 10° min^{-1}.

In-situ XRD patterns were collected on an X'Pert Pro MPD diffractometer equipped with an in-situ cell that allows heating and the introduction of gases. The diffractometer was operated at 40 kV and 40 mA using Cu-$K\alpha$ radiation source. To trace the structural

changes of the catalyst, the sample was heated up to 500 °C under the flow at 20 mL min^{-1} of 5 vol.% H_2/N_2, during which the XRD patterns were recorded at 28 (RT, room temperature), 50, 100, 200, 300, 400 and 500 °C, respectively. Then, the catalyst was cooled to RT under the N_2 atmosphere and the XRD patterns were also recorded.

2.2.2. Electrochemical measurements

The electrochemical characteristics of the prepared catalysts were tested in a cell consisting of a three-electrode system in 0.1 M perchloric acid ($HClO_4$) at 25 °C. A reversible hydrogen electrode (RHE) was used as the reference electrode and a platinum wire was used as the counter electrode. The measurements were carried out using a rotating disk electrode (RDE; Pine, 5908 Triangle Drive, Raleigh, NC 21617).

To prepare an electrode, the uniform suspension was made by mixing 2 mg of as-synthesized catalyst with 1 mL of methanol/Nafion® (5 wt%) solution (30:1 wt%) and ultrasonic oscillated for 30 min. 10 μL of the catalyst suspension was transferred to the polished glassy carbon (GC) disk electrode (0.283 cm^2) and dried in air for 15 min. For the LSV experiment, the electrolyte was saturated with O_2 and operated at rotation speed of 1600 rpm at 5 mV s^{-1} from 0 to 1.2 V.

2.3. Single cell performance measurement

The single cell (50 cm^2) test was performed under the steady-state conditions of the fuel cell on the single cell test batch (Green Light). I–V discharge characteristics were measured to test the effect of the catalyst on the performance of the fuel cell. The stoichiometry of H_2 and air was kept constant at 1.2 and 2.5, respectively. The pressure of both gas inlets was fixed at 60 kPa (In this article, the operation conditions were all expressed by gauge pressure). The operation temperature was set at 75 °C and the relative humidity (RH) of both H_2 and air was 80%.

40% Pt/C (JM) and Co@Pt (1:3)/C (reduced) catalysts were respectively used as the anode and cathode catalysts. The catalyst ink was sprayed directly onto the 212 Nafion membranes at 80 °C to form the catalyst layer. The ink was prepared by mixing catalyst with a solution of 5 wt% Nafion (Dupont), iso-propanol and then sonicated for 4 h. In the cathode side, the loading of the as-prepared catalyst was 0.36 mgPt cm^{-2}, and the loading of catalyst in anode was 0.2 mgPt cm^{-2}. The ratio of electrocatalyst to Nafion was 3:1. Then, the MEA was followed by the simply physically placing gas diffusion layers (GDLs) (SGL Company) without the need for a hot-pressing process. For comparison, a single cell test was also carried out in which the MEA was fabricated with 40% Pt/C (JM) catalyst. The loading of Pt metal was 0.4 mgPt cm^{-2} in the cathode and 0.2 mgPt cm^{-2} in the anode.

2.4. Stability of the single cell performance

The durability and reliability are of major concerns for the development of the catalysts employed in fuel cell. In order to estimate the durability of the as-prepared catalyst, experiment was devoted to the operation of a single cell for 130 h in the stationary current conditions. The stoichiometry of H_2 and air was kept constant at 1.2 and 2.5, respectively. The pressure of both gas inlets was fixed at 60 kPa. The operation temperature was 75 °C and the RH of both H_2 and air was 80%. Current–voltage (I–V) curves, CV curves and EIS spectra were measured to trace the performance of the cell as a function of time.

2.5. Electrochemical impedance spectroscopy (EIS) measurement

EIS measurements of the fuel cell were carried out using a VMP2/Z workstation at galvanostatic mode under a constant load of 5 A with a frequency ranging between 10 kHz and 100 mHz. All impedance spectra reported herein were measured between the fuel cell cathode and anode. Air was passed through the tested electrode and hydrogen was passed through the counter electrode. Pt/C (JM) or Co@Pt/C was respectively used as the working electrode and Pt/C used as the counter electrode. A series of impedance measurements at periodic time intervals were recorded during the experiment applying a sine wave distortion (AC perturbation) of 500 mA amplitude. Fuel cell was operated at 75 °C and the pressure of the gases inlets was 60 kPa and the RH (both H_2 and air) was 80%.

2.6. Cyclic voltammograms measurements

CV measurements were carried out in order to compare the losses of the electrochemical surface area (ECSA) of the electrodes during the stability testing. During the CV measurements, nitrogen was fed to the working electrode (cathode) and hydrogen was fed to the counter electrode (anode side). The counter electrode was also used as the reference electrode because of the negligible over potential of hydrogen oxidation and reduction. The potential was scanned from 0.05 V to 1.15 V versus the reversible hydrogen electrode (RHE) at a rate of 20 mV s^{-1}. The ECSA was evaluated from the hydrogen desorption peaks of the CV curve.

3. Results and discussion

3.1. TEM and XRD analyses

Fig. 1 shows the HR-TEM images of Co@Pt (1:3)/C (reduced) electrocatalyst. The different brightness indicates that there exists dissimilar element on the carbon support. The core–shell components of Co@Pt (1:3) are easily differentiable by the TEM images because of the strong imaging contrast between Co and Pt. High-resolution images show a different morphology of two isolated elements of different colors on the carbon support. The distinctive

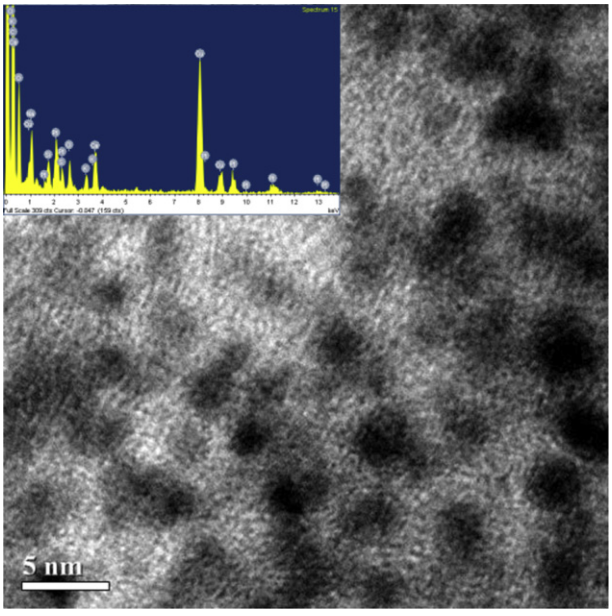

Fig. 1. HR-TEM and EDX images of Co@Pt (1:3)/C (reduced) electrocatalyst.

images show that the core of the Electron micrographs is closely covered by other elements, which is clearly shown by the different color. EDX (Energy-dispersive X-ray spectroscopy) is directly applied to these particles. The results show that the surface of Cobalt elements might be covered by the Pt element. The core of the images is ascribed to the Cobalt element, while the surface of the element is ascribed to Pt element. This suggests that the surface of Co of Co@Pt/C (1:3) is completely covered by the Pt over-layers. This superior structure and excellent dispersion of the metal nanoparticles might contribute to the superior adsorption and the activation of oxygen molecules on the surface of Pt, which caused the enhancement of the activity of the Co@Pt/C catalysts for oxygen reduction reactions. It will be discussed below.

Fig. 2 shows the TEM images of Co@Pt/C of different Co:Pt ratios, in which appears polycrystalline rather than single crystal. Especially the discern diffraction images are in discontinuous cycles. It is seen that metal particles are uniformly dispersed on the surface of carbon and there is no obvious aggregation of Pt particles. The

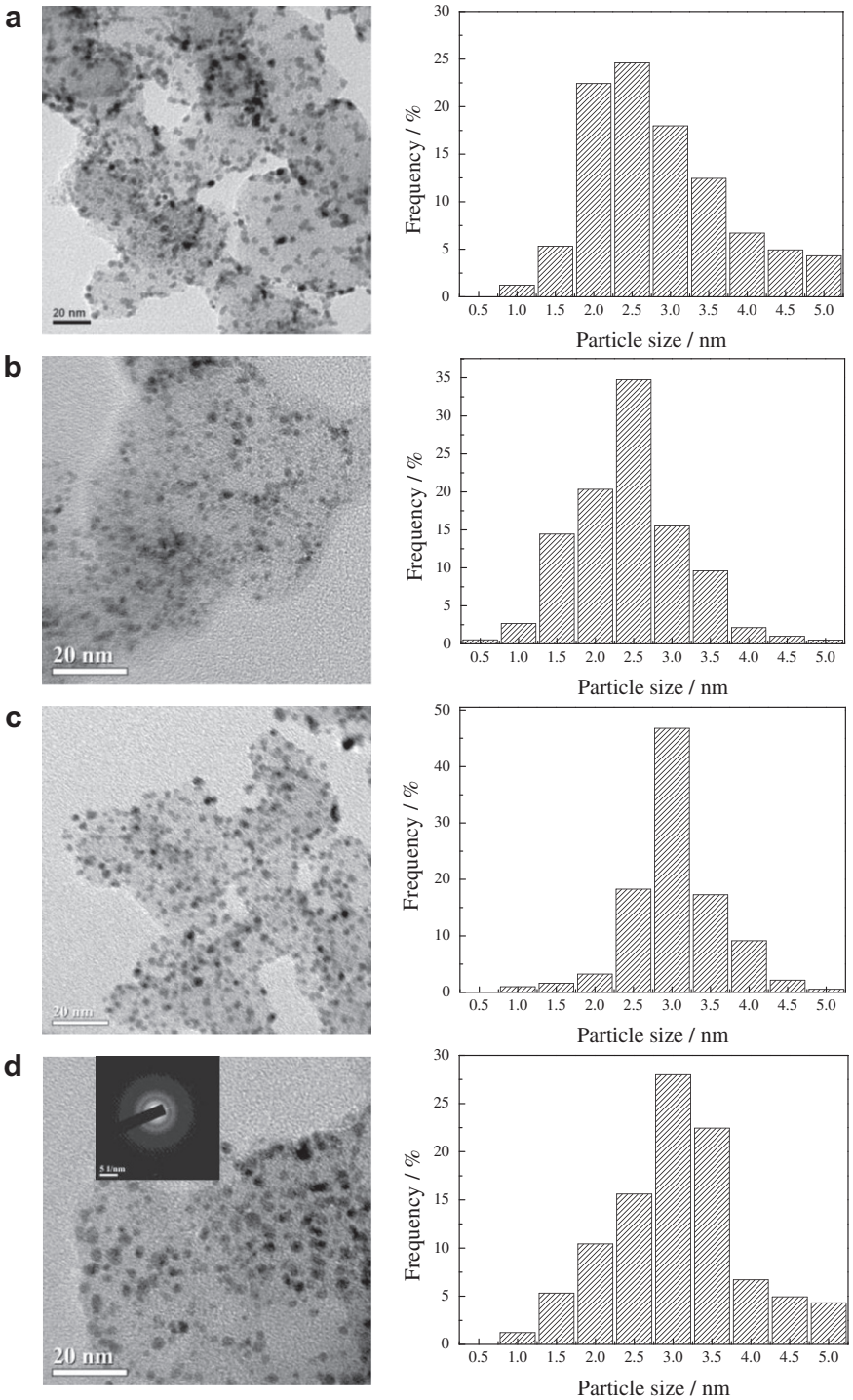

Fig. 2. TEM images and particles size distributions of: (a) Pt/C (JM); (b) Co@Pt (1:3)/C; (c) Co@Pt (1:3)/C (reduced) and (d) Co@Pt (1:1)/C (reduced) electrocatalysts.

Table 1
Mean crystallite sizes of Pt/C (JM) and Co@Pt/C obtained from XRD and TEM.

Catalyst	Mean crystallite size (nm)	
	XRD[a]	TEM
Pt/C (JM)	3.5	2.8
Co@Pt (1:3)/C (reduced)	3.8	3.0
Co@Pt (1:3)/C	2.7	2.4
Co@Pt (1:1)/C	3.8	3.1

[a] The mean particle size was calculated from Pt (111) peak according to Scherrer's equation.

Table 2
Particle sizes of Co@Pt (1:3)/C at different temperature obtained from in-situ XRD.

Temperature (°C)	Peak broadening (FWHM)	Particle size (nm)
28	4.008	2.09
50	3.571	2.34
100	3.471	2.40
200	3.405	2.46
300	3.042	2.75
400	2.544	3.29
500	2.248	3.72
Cool down to 28	2.233	3.76

particle size of Pt/C catalyst, Co@Pt/C (1:3), Co@Pt/C (1:3, reduced) and Co@Pt/C (1:1, reduced) were listed in the Table 1, which were respectively at 2.8, 2.4, 3.0 and 3.1 nm. It means the average size of the particles of reduced sample grew larger than that of the fresh ones. The ratio of Co to Pt did not affect the particle size of Co@Pt very much, while it is reported that the size of the particle has a great influence on the performance of electrocatalysts. The most optimal particle size distribution is 3–5 nm. The catalyst at the particle size less than 3 nm did not contribute much to the specific activity and the specific surface area. Small Pt nanoparticles were found to be frequently incorporated into the micropores, and thus appeared to be covered by a thin carbon layer and embedded into the carbon matrix [16]. Another tendency which could be seen through the images is that with the increasing of the content of Co, the size of catalyst particles got larger.

The XRD patterns of Pt/C (JM), series of as-prepared Co@Pt/C and Co/C catalysts are respectively shown in Fig. 3. It was found that no diffraction peaks of cobalt were detected in the Co@Pt/C catalysts. The diffraction peaks are respectively at 39, 46, 67, and 81° of 2θ, which are respectively assigned to (111), (200), (220) and (311) crystal face of Pt metal. The resultant diffraction patterns indicated that Pt catalysts are face-centered cubic structure and the particle size of Pt was calculated using Debye–Scherrer equation by fitting the Pt (111) peak.

$$\left(L = \frac{0.94 \times \lambda_{K\alpha 1}}{B_{(2\theta)}\cos\theta_B}\right)$$

Where L is the average particle size, $\lambda_{K\alpha 1}$ is the X-ray wave length, θ_B is the angle of the Pt (111) peak and $B_{(2\theta)}$ is the peak broadening (FWHM). The particles size of Co@Pt (1:3)/C (reduced), Co@Pt (1:1)/C (reduced), Co@Pt (1:3)/C, Co@Pt (1:1)/C and Pt/C (JM) were found to be respectively at about 4.8, 4.5, 2.8, and 3.9 nm (Table 2). The differences between the mean particle sizes obtained by TEM and XRD techniques could be attributed to the fact that XRD technique only reflects the crystalline particles, but not the actual morphology of the catalysts as described above.

The diffraction peaks of the cobalt and carbon for the Co/C particles were respectively at 26° and 44.7°, which were assigned to C (002) and Co (002) crystal face. The diffraction peak of Co (002) was wide and quite weak, which might be due to the amorphous or the low content of Cobalt. When the Pt was added, there is no diffraction peak of cobalt for the Co@Pt/C catalysts. It means that Co (002) peak disappeared for series of Co@Pt/C catalyst samples. While for the Pt–Co alloy catalyst, the Co diffraction peaks could be discovered [17]. Combined with the results of HR-TEM images of Co@Pt/C samples (Fig. 1), it might be due to the coverage of Cobalt by Pt and thus the formation of core–shell structured for Co@Pt/C samples. The formation of core–shell structure makes the coverage of Co by Pt, which could be helpful to prevent the leach of the Co ions.

To trace the changes of as-prepared Co@Pt/C nanostructure during the high-temperature reduction and optimize the heat treatment temperature, we conducted in-situ XRD examinations of the catalyst in mixture atmosphere (5% H_2 and 95% N_2) with elevating temperatures. As shown in Fig. 4, No cobalt species were detected, suggesting that the cobalt species, most probably existing as CoO_x, are amorphous or their particle sizes are too small to be detected by XRD [18]. With increasing the treatment temperature of the reduction atmosphere, still no cobalt species could be found.

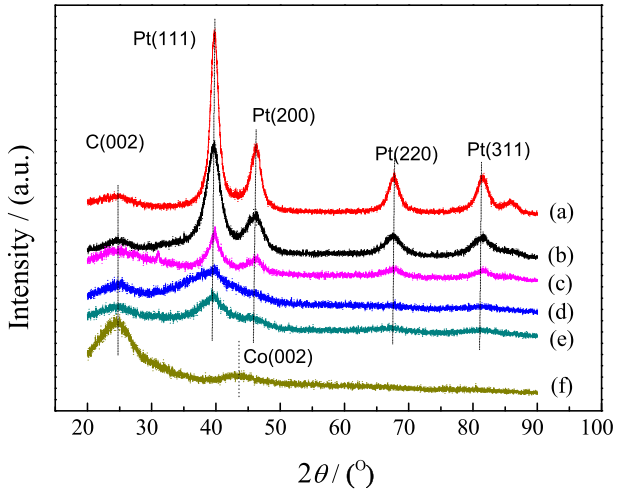

Fig. 3. XRD patterns of Pt/C, Co/C and as-prepared Co@Pt/C samples: (a) Co@Pt (1:3)/C (reduced); (b) Pt/C (JM); (c) Co@Pt (1:1)/C (reduced); (d) Co@Pt (1:3)/C; (e) Co@Pt (1:1)/C and (f) Co/C.

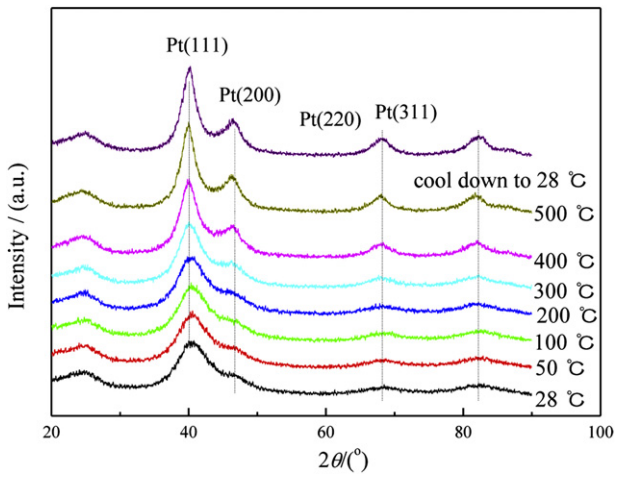

Fig. 4. In-situ XRD patterns of the as-calcined Co@Pt/C catalyst with increasing reduction temperature under the mixture atmosphere (5% H_2 and 95% N_2, volume ratio).

It proved that the Pt was deposited onto the surface of Co particles and core shell nanoparticles were formed. The width of the diffraction peak got gradually narrowed and the intensity of Pt diffraction peaks became sharp when the temperature was lower than 400 °C, indicating that the particles were larger than that of fresh catalysts and some amorphous Pt transferred into crystalline phase. The changes of particles size of the catalysts during the heat treatment are listed in the Table 2. When the sample was cooled down to room temperature (about 28 °C) after 500 °C treatment, the diffraction pattern was similar to the one at 500 °C, which indicated that the structural change of the Co@Pt/C nanoparticles was irreversible.

3.2. Electrochemical performances

In order to characterize the oxygen reduction activity in the electrolyte solution, we used herein the Co@Pt/C catalyst of different Co/Pt ratios and commercial Pt/C (JM) catalysts in O_2-saturated 0.1 M $HClO_4$. The obtained linear sweep voltammograms are shown in Fig. 5. It is found that the content of cobalt in Co@Pt/C catalysts retain their ORR activity crucial for fuel cell catalysts. The Co@Pt (1:3)/C (reduced) shows the best oxygen reduction reaction properties, which is even higher than that of Pt/C (JM). The half-wave potential of Co@Pt (1:3)/C (reduced) shifts about 8 mV toward the positive direction compared with that of Pt/C (JM) catalysts. At the ratio of 1:1 for Co:Pt, the ORR activity is poorer than that of Pt/C (JM). The ORR activity of for the Co@Pt (1:3)/C (reduced) catalyst is higher than that of Pt/C (JM).

From the results of the LSV curves, it was deduced that the improved mass activity of platinum might be due to the effect of the geometric effect induced by the formation of core–shell structure. This allows a larger number of catalytically active sites to be present on the accessible surface of the particles as cobalt played as contained in the underlying core. Furthermore, the inter-atomic Pt–Pt distances in the Co@Pt/C catalysts might be changed, which can result in more facile oxygen adsorption and oxidation due to the modified surface and electronic properties [19]. The promotion of catalytic activity of Co@Pt/C might be due to the synthetic effect between cobalt and platinum during the activation process.

The LSV curves also indicate that catalyst after heat-treatment shows better performance comparing to the one without heat treatment. The half-wave potential of Co@Pt (1:3)/C is 0.803 V. Compared with Co@Pt (1:3)/C catalyst, the ORR performance of Co@Pt (1:3)/C (reduced) catalyst improves obviously. The half-wave potential of Co@Pt (1:3)/C (reduced) catalyst could reach to 0.842 V. The ORR activity of the series catalysts are in the sequence of Co@Pt (1:3)/C (reduced) > Pt/C (JM) > Co@Pt (1:3)/C (Table 3).

Table 3
The mass activity@0.9 V of the catalysts calculated from Fig. 5.

Catalyst	Mass activity@0.9 V (mA mg^{-1} Pt)
Pt/C (JM)	35.2
Co@Pt (1:1)/C	15.0
Co@Pt (1:1)/C (reduced)	35.5
Co@Pt (1:3)/C	21.2
Co@Pt (1:3)/C (reduced)	50.3

Combined with the results of the in-situ XRD, it shows that at the reduction temperature lower than 300 °C, the particle size of Pt does not change much and the higher temperature treatment favors for the formation of Pt crystalloid in reduction condition.

Tafel plots of Co@Pt (1:3)/C (reduced), Co@Pt (1:3)/C and Pt/C catalyst are shown in Fig. 6. It is found that at high potential (above 0.9 V) the obtained Tafel slopes for the Pt/C, Co@Pt (1:3)/C (reduced) and Co@Pt (1:3)/C are 74, 78 and 85 mV $decade^{-1}$, respectively. It can be concluded that the reaction pathway and the rate determining step were principally the same for all the electrocatalysts studied here.

3.3. Single cell performance and in-situ electrochemical analysis

The performance of single cell of Co@Pt (1:3)/C (reduced) as cathode electro-catalyst and the commercial Pt/C (JM) catalyst as anode in single PEM fuel cell was shown in Fig. 7. We can see that the open-circuit potential was 0.97 V when the Co@Pt/C catalyst was applied to the cathode. The MEA fabricated with Pt/C catalyst (as cathode electrode) gave a slightly higher cell performance compared with the one using Co@Pt/C catalyst as the cathode under the same measuring conditions. The single fuel cell generates a maximum power density of 475 mW cm^{-2} at 0.475 V.

EIS (Electrochemical impedance spectroscopy) is a powerful diagnostic testing method for fuel cells because it is non-destructive and provides some useful information about fuel cell performance [20]. EIS was used to measure the intrinsic properties of the electrodes which were caused by the catalyst in this experiment, such as ohmic resistance, charge-transfer resistance and

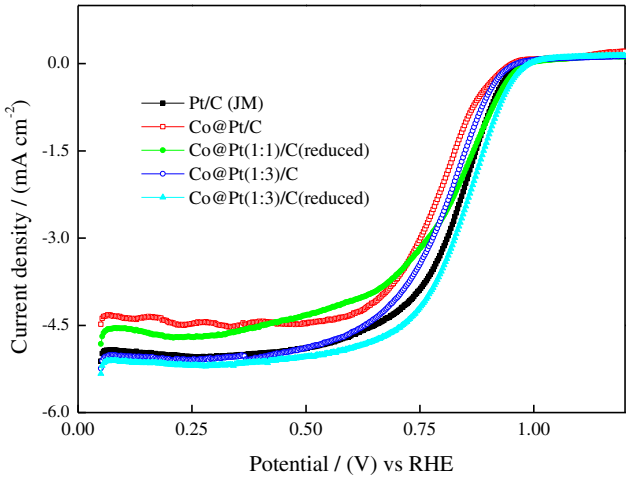

Fig. 5. Linear sweep voltammograms (LSVs) of O_2 reduction on Co@Pt/C and commercial Pt/C (JM) catalysts in O_2-saturated 0.1 M $HClO_4$ at room temperature. Sweep rate: 5 mV s^{-1}, rotation speed was 1600 rpm.

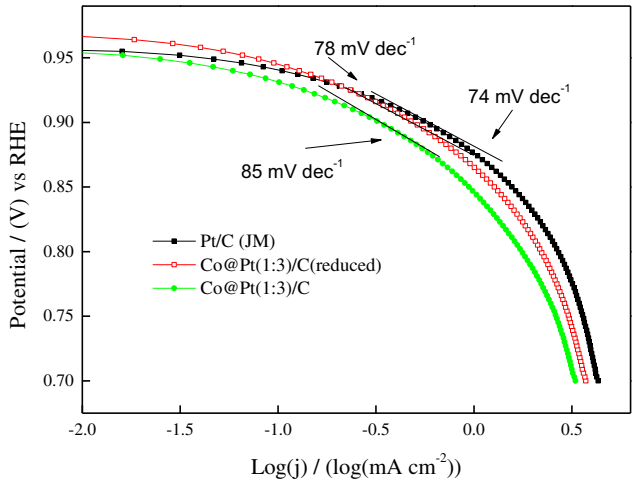

Fig. 6. Tafel plots for the ORR on Pt/C (JM) and as-prepared electrocatalysts in O_2-saturated 0.1 M $HClO_4$ at room temperature.

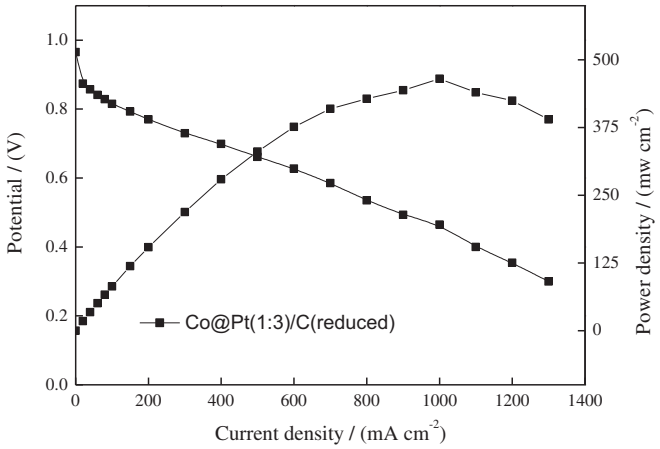

Fig. 7. Single-cell performance of Co@Pt (1:3)/C (reduced) as cathode electrocatalyst, anode and cathode temperature was both 75 °C, the stoichiometry for air and hydrogen was 2.5 and 1.2 respective, the pressure of both gas inlet was 60 kPa, the relative humidity (RH) of air and hydrogen was both 80%, the active area was 50 cm^2.

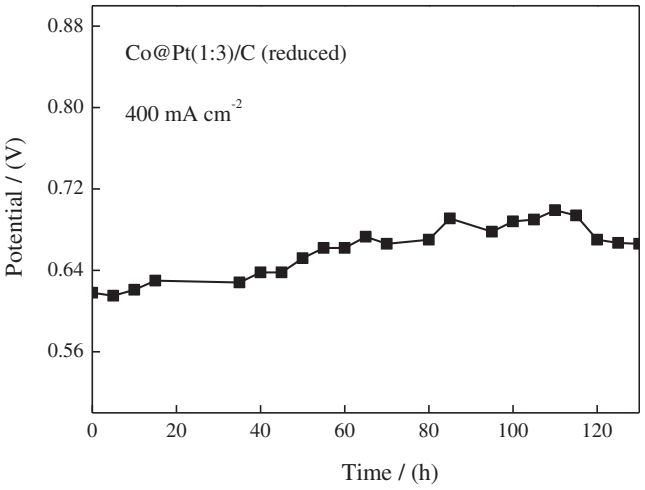

Fig. 9. Lifetime evaluation of as-prepared electrocatalyst for oxygen reduction in single cell, current density 400 mA cm^{-2}, cell temperature 75 °C, and gas inlet pressure was 60 kPa.

mass-transfer resistance in the catalyst layer. Nyquist plots of EIS may include one, two, or three arcs: low, medium, and high frequency loops. These loops are related to the mass transport resistance, charge transfer resistance combined with double layer capacitance within the catalyst layer, and the structural features of MEA, respectively [21]. However, in some researches, the internal ohmic resistance and the contact capacitance in the granular electrode structure has been stated to be responsible for the high frequency loop [22].

EIS measurement was performed as described in Fig. 8, which is the Nyquist representation of EIS measurements of single cell. Pt/C (JM) and Co@Pt (1:3)/C (reduced) was respectively used as working electrode and Pt/C counter electrode, both of which were supplied with neat H_2. The high frequency (HF) interception on the real impedance axis of the Nyquist plot represents ohmic resistance of the cell (RHF), which contains the ohmic resistance of the cell components, such as the membrane, catalyst layer, backing layer, end plate, as well as the contact resistance between each of them [23]. The ohmic resistance of the fuel cell using Pt/C (JM) is about 10.1 mΩ, while that of Co@Pt (1:3)/C (reduced) catalyst is 13.9 mΩ.

The diameter of the kinetic loop, which corresponds to the charge-transfer resistance of fuel cell, deduced as the difference between low frequency and high frequency intercepts of the curve with Re/Z/axis, was at 12.0 and 12.2 mΩ for Pt/C (JM) and Co@Pt (1:3)/C (reduced) catalyst, respectively. It was found that the nearly semicircle only shifted little along the Re/Z/axis by the ohmic resistance of the cell between Pt/C (JM) and Co@Pt (1:3)/C (reduced) catalyst. In short, the above results can be interpreted as that the addition of cobalt did not make the ohmic resistance and charge-transfer resistance of the cell increase much.

Fig. 9 shows the stability of single cell with Co@Pt/C as the cathode catalyst operated at 400 mA cm^{-2}. It was found that during the first 40 h operation, the performance of the fuel cell increased a little. After that, the performance kept stable. The decay of the performance was not significant during the 130 h operation process.

The polarization curves (Fig. 10) of the MEA which employed Co@Pt/C catalyst as the cathode also show the same fact that during the 110 h' operation, the performance improved gradually, and then slight decay happened to the cell. During the whole aging test, the

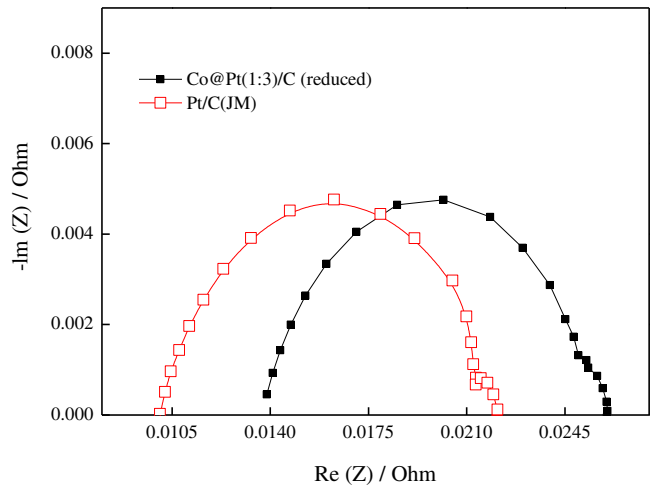

Fig. 8. Nyquist representation of electrochemical impedance spectroscopy (EIS) measurements results of single cell, as-synthesized Co@Pt (1:3)/C (reduced) catalysts used as working electrode.

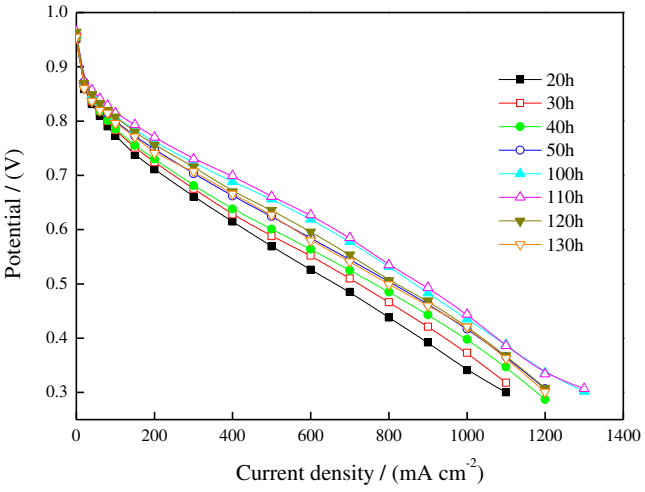

Fig. 10. Polarization curves of a single cell using Co@Pt (1:3)/C (reduced) catalyst, anode and cathode temperature was both 75 °C, the stoichiometry for air and hydrogen was 2.5 and 1.2 respective, the pressure of both gas inlet was 60 kPa, the relative humidity (RH) of air and hydrogen was both 80%, the active area was 50 cm^2.

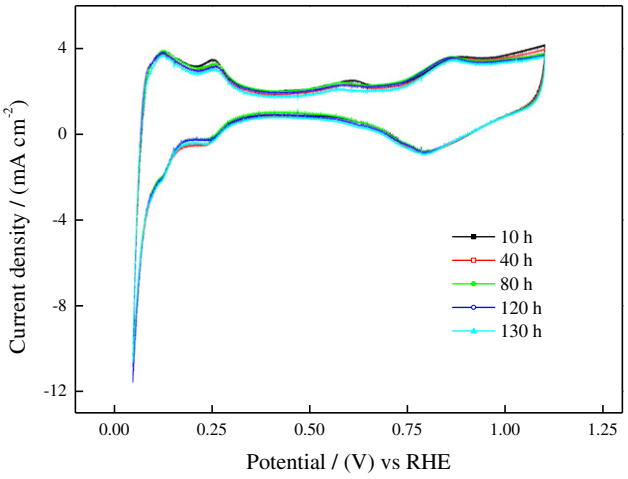

Fig. 11. Cyclic voltammograms of MEA using Co@Pt (1:3)/C (reduced) catalyst potential scan rate 20 mV s^{-1} at different running time, anode and cathode temperature was both 75 °C, the stoichiometry for air and hydrogen was 2.5 and 1.2 respective, the pressure of both gas inlet was 60 kPa, the relative humidity (RH) of air and hydrogen was both 80%, the active area was 50 cm^2.

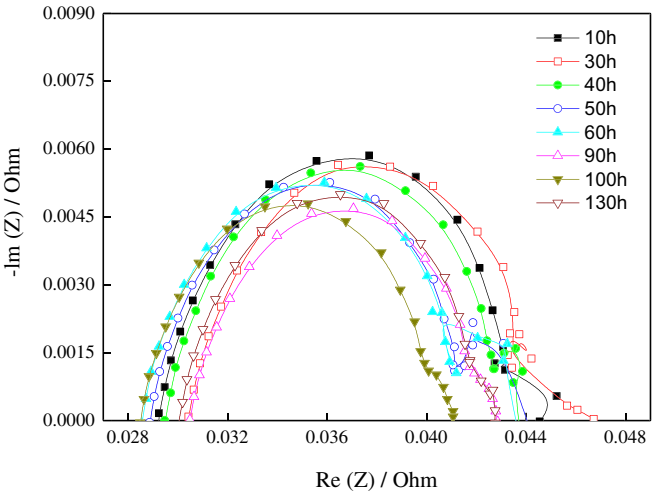

Fig. 12. Electrochemical impedance spectra of the fuel cell at different running time, anode and cathode temperature was both 75 °C, the stoichiometry for air and hydrogen was 2.5 and 1.2 respective, the pressure of both gas inlet was 60 kPa, the relative humidity (RH) of air and hydrogen was both 80%, the active area was 50 cm^2.

decay of the cell is slow and inconspicuous. It infers that the durability of Co@Pt core shell structure catalyst is superior to that of alloys.

A larger number of accessible electrochemically active sites provide the contribution to the increased ORR activity and the improved performance of fuel cell. CV curves collates closely with the performance of the single cell. CV techniques were operated to detect the variation of the electrochemically active surface areas (ECSA) with operation time (Fig. 11). The values of the ECSA were calculated from CV data and the results are provided in Table 4. It was found that ECSA increased at the first 40 h (ECSA reached 53.9 $m^2\ g^{-1}$ Pt), after that, it kept quite stable. The obvious decay of ECSA appeared after 130 h operation (ECSA decreased to 51.1 $m^2\ g^{-1}$ Pt).

It is clear that the activity of the fuel cell is consistent with the electrochemical active surface area. The increasing of ECSA in the first 30 h is most likely due to the activation of MEA. The activation process of MEA is not only a humidifying process of proton exchange membrane, but also a complex process including the construction of transport channels for electron, proton, gas and water and the optimization of electrode structure [24]. According to CV curves, the loss of the overall ECSA of Co@Pt/C might be due to the aggregation of Pt particles.

Fig. 12 shows the change of the EIS curves of fuel cell during operation for 130 h the charge transfer resistance was 15.5 mΩ at the first 10 h' operation. However, it decreased to 14.0, 13.5, and 12.3 mΩafter 40, 50 and 90 h operation, respectively. It can be seen that with the increase on operation time, the charge transfer resistance which has a strong impact on the fuel cell performance decreased. However, after 100 h operation, with time going on, the charge transfer resistance of Co@Pt/C catalyst increased. It reached 12.4 mΩ at 100 h and 12.8 mΩ at 130 h, which might be due to the decay of the catalyst.

It can be seen that with the operation time increasing, the ohmic resistance decreased, which might be caused by the activated surface area of the catalyst. During the activation process, the electrochemical reaction resistance of oxygen electrode decreased. The activation process enhanced the effective area of MEA, and thus it is favorable to improve the performance of fuel cell [25]. However, with operation time continued, the charge transfer resistance began to increase, which might be due to the decay of the catalyst.

Table 4
Electrochemical surface areas of Co@Pt (1:3)/C (reduced) catalysts from CV curves in Fig. 11.

Operation time (hours)	(mC cm^{-2})	ECSA ($m^2\ g^{-1}$ Pt)
10	16.14	53.4
40	16.31	53.9
80	16.05	53.1
120	15.89	52.5
130	15.47	51.1

4. Conclusions

The as-prepared Co@Pt nano-particles are in core shell structure and the particles size is mainly distributed at the range of 3–5 nm. Results of in-situ XRD show that the heat treatment favors for the formation of crystalline structure and the proper particle size of catalyst, which might contribute to the improvement of the catalyst performance. The proper temperature for heat treatment is 300–400 °C. From the electrochemical measurements, the formation of core–shell structure favors for decreasing the content of Pt and improving the performance of the fuel cell. Applying Co@Pt/C catalysts as the cathode electrode of the single fuel cell, the cell generates a maximum power density of 475 mW cm^{-2} at 0.475 V. The formation of the core–shell structure of Co@Pt/C catalyst is favorable to improve the stability, which can be proved by durability testing and electrochemical characterization. The active surface area of catalyst did not change much after 130 h operation, which could be also identified by the EIS results. Different from alloy Pt-M catalyst, the coverage of Cobalt by Pt helps prevent the dissolution of cobalt during the real operation process, which gives a much more stable performance.

Acknowledgments

The authors gratefully acknowledge the financial support from National Natural Science Foundation of China (No. 20703031), the Doctoral Program of Higher education (No. 20070247055), Program for Young Excellent Talents in Tongji University (No. 2006KJ022), Shanghai Leading Academic Discipline Project (No. B303) and 111 Project (No. B08019).

References

[1] J.H. Wee, K.Y. Lee, S.H. Kim, J. Power Sources 165 (2007) 667–677.
[2] R. Othman, A.L. Dicks, Z.H. Zhu, Int. J. Hydrogen Energy 37 (2012) 357–372.
[3] M.K. Min, J. Cho, K. Cho, H. Kim, Electrochim. Acta 45 (2000) 4211–4217.
[4] L. Carrette, K.A. Friedrich, U. Stimming, Fuel Cells 1 (2001) 15–39.
[5] P. Mani, R. Srivastava, P. Strasserc, J. Power Sources 196 (2011) 666–673.
[6] Q.M. Xu, E. Kreidler, T. He, Electrochim. Acta 55 (2010) 7551–7557.
[7] S.C. Zignani, E. Antolini, E.R. Gonzalez, J. Power Sources 182 (2008) 83–90.
[8] S. Kalele, S.W. Gosavi, J. Urban, S.K. Kulkarni, Curr. Sci. 91 (2006) 1038–1052.
[9] Y. Ma, H. Zhang, H. Zhong, T. Xu, H. Jin, X. Geng, Catal. Commun. 11 (2010) 434–437.
[10] Y. Zhao, X. Yang, J. Tian, F. Wang, L. Zhan, Int. J. Hydrogen Energy 35 (2010) 3249–3257.
[11] B.J. Jankiewicz, D. Jamiola, J. Choma, M. Jaroniec, Adv. Colloid Interface Sci. 170 (2012) 28–47.
[12] N. Kristian, Y.L. Yu, J.M. Lee, X.W. Liu, X. Wang, Electrochim. Acta 56 (2010) 1000–1007.
[13] J.X. Wang, H. Inada, L.J. Wu, Y.M. Zhu, Y.M. Choi, W.P. Zhou, R.R. Adzic, J. Am. Chem. Soc. 131 (2009) 17298–17302.
[14] M.H. Lee, J.H. Do, J. Power Sources 188 (2009) 353–358.
[15] S.B. Liu, J.N. Yuan, Z.L. Zhang, D.H. Duan, Y.B. Li, X.G. Hao, Chin. J. Inorg. Chem. 26 (2010) 1171–1176.
[16] L. Gan, H.D. Du, B.H. Li, F.Y. Kang, New Carbon Mater. 25 (2010) 53–59.
[17] K. Jayasayee1, J.A.R.V. Veen, T.G. Manivasagam, S. Celebi, E.J.M. Hensen, F.A.D. Bruijn, Appl. Catal. B Environ. 111-112 (2012) 515–526.
[18] X.Y. Liu, A.Q. Wang, L. Lin, T. Zhang, C.Y. Mou, J.F. Lee, J. Catal. 278 (2011) 288–296.
[19] E.I. Santiago, L.C. Varanda, M.J. Villullas, J. Phys. Chem. C 111 (2007) 3146–3151.
[20] C.J. Xie, S.H. Quan, Procedia Environ. Sci. 11 (2011) 589–596.
[21] T. Romero-Castañón, L.G. Arriaga, U. Cano-Castillo, J. Power Sources 118 (2003) 179–182.
[22] A. Fischer, J. Jindra, H.J. Wendt, Appl. Electrochem. 28 (1998) 277–282.
[23] B. Li, R. Lin, D.J. Yang, J.X. Ma, Int. J. Hydrogen Energy 35 (2010) 2814–2819.
[24] K. Zhu, Y.X. Chen, Z.Q. Han, J.Y. Zhang, Y.B. Sun, Chin. J. Power Source 26 (2002) 267–268. 325.
[25] K. Zhu, J.Y. Zhang, Z.Q. Shan, Y.X. Chen, Chin. J. Power Sources 30 (2006) 41–43. 13.